

Unifying Atoms and Colloids near the Glass Transition through Bond-Order Topology

Laura Stricker^{1,*}, Peter M. Derlet^{2,†}, Ahmet Faik Demirörs³, Hanumantha Rao Vutukuri⁴, and Jan Vermant¹

¹*Department of Materials, ETH Zürich, 8093 Zürich, Switzerland*

²*Laboratory for Theoretical and Computational Physics, Paul Scherrer Institut, 5232 Villigen PSI, Switzerland*

³*Department of Physics, University of Fribourg, 1700 Fribourg, Switzerland*

⁴*Active Soft Matter and Bio-inspired Materials Lab, Faculty of Science and Technology, University of Twente, MESA+ Institute, 7500 AE Enschede, The Netherlands*

 (Received 25 July 2022; revised 4 January 2024; accepted 2 April 2024; published 24 May 2024)

In this combined experimental and simulation study, we utilize bond-order topology to quantitatively match particle volume fraction in mechanically uniformly compressed colloidal suspensions with temperature in atomistic simulations. The obtained mapping temperature is above the dynamical glass transition temperature, indicating that the colloidal systems examined are structurally most like simulated undercooled liquids. Furthermore, the structural mapping procedure offers a unifying framework for quantifying relaxation in arrested colloidal systems.

DOI: [10.1103/PhysRevLett.132.218202](https://doi.org/10.1103/PhysRevLett.132.218202)

Colloidal systems have been successfully used as a convenient microscopic model for atomistic systems [1], as demonstrated by studies on both crystalline [2] and glassy systems [3,4]. Compared to their atomic counterparts, micrometer-sized systems offer the advantage of direct real-space visualization through microscopy imaging. However, despite the large body of work based on the paradigm of “colloids-as-big-atoms” for equilibrium phase transitions [5,6], the equivalence has not been established as clearly for more challenging conditions, such as far-from-equilibrium or time-dependent dynamics. In this respect, the long-time dynamics close to the glass transition provides an interesting test case, that has been studied both theoretically, with the mode coupling theory (MCT) [7], and experimentally [8,9], and continues to be employed [10–13]. Still, quantitative mapping of colloidal systems onto atomistic ones remains limited due to the ambiguity in determining the glass transition volume fraction [14].

The glass transition, both in colloidal suspensions and atomistic glass formers, is characterized by large increases in relaxation time [15] and viscosity [16] as the system dynamically arrests [17,18]. Interestingly, the microscopic dynamics are fundamentally different, i.e., Brownian versus Newtonian, as well as the dissipative mechanisms, since the interaction of colloids with the suspending medium dampens thermal fluctuations. Nevertheless, a nominally similar structural relaxation emerges [19,20], due to the timescale separation of slow local density fluctuations and the fast microscopic dynamics [21–24]. Because of crowding, caging mechanisms appear through cooperative rearranging of particles with their nearest neighbors [24]. Hence, a variety of short-range ordered arrangements originate that minimize the local potential energy, the so-called “locally favored structures” (LFS) [25]. The development of LFS

when approaching the glass transition is however limited by the geometric constraints posed by an Euclidean space [26]. In three dimensions, full tiling with maximally symmetric polyhedra (icosahedra) is not achievable and other defected topological structures emerge, such as the Frank-Kasper motifs [27,28]. The situation is quite different in two dimensions, where minimally frustrated triangles can be tiled in a space filling way [29], leading to fundamental differences between 2D and 3D glasses [30].

The geometric frustration, which occurs in three dimensions, originates from a competition between locally and globally favourable energetic configurations and ultimately prevents crystallization. Fragments of topologically close-packed Frank-Kasper (FK) phases have been observed in simulations both in undercooled liquids [31] and in soft-particle systems [32]. A comprehensive topological framework of the glass transition based on the homotopy of the icosahedral point-symmetry group was developed by Nelson [33,34], allowing for the enumeration of structural motifs based on the algebra associated to the SU(2) group, and has recently been successfully applied to describe simulated model atomistic systems [35]. Compared to other LFS descriptions, such a framework provides an intrinsic link between local, midrange, and global ordering [36]. This topological description is also able to reconcile the kinetic and the structural views of the glass transition. Recent work has shown that relaxation processes in binary model glasses are intimately related to the evolution of such structural motifs, where even the localized stringlike structural excitation seen in both glasses and undercooled liquids [37] can be rationalized in terms of a re-arrangement of the disclination network describing the defected topological structure [38,39].

In the present work, we exploit this structural perspective to establish a mapping between binary colloidal mixtures, compressed with an electric field (a system controlled by volume fraction), to atomistic simulations of an undercooled liquid undergoing temperature quenching. The agreement in the populations of structural motifs is excellent, suggesting their independence on the details of the interaction potential. In particular, our findings reveal that the “arrested” experimental systems align with simulated temperatures exceeding the glass transition point. Slower compressions correspond to lower simulated mapping temperatures. In essence, our Letter provides a clear and unambiguous method to quantify relaxation in colloidal systems.

Experiments and simulations.—Experiments are carried out using a binary colloidal particle suspension whose concentration is controlled through dielectrophoretic forces generated by an electric field gradient (“dielectrophoretic bottle” [40]). A sketch of the experimental setup (Supplemental Material, Figs. 1 and 2) and additional details can be found in the Supplemental Material, Secs. A–D [41]. We use binary mixtures of sterically stabilized polymethyl methacrylate (PMMA) colloidal particles with diameters of 3.0 and 3.6 μm and a 5% polydispersity, giving a ratio $\alpha = 0.84 \pm 0.02$, and a dielectric constant $\epsilon_p \approx 2.6$ [52]. The small and large particles are covalently labeled with the fluorescent dye 7-nitrobenzo-2-oxa-1,3-diazol (NBD) and Nile blue oxazone (Nile red), respectively, and sterically stabilized with poly(12-hydroxystearic acid) [53]. An additional radii ratio $\alpha = 0.7 \pm 0.06$ is achieved with particle diameters 2.1 and 3 μm with a polydispersity of 4% and 5%, respectively, where the large particles are dyed with rhodamine isothiocyanate (RITC). The particles are dispersed in equal weight parts in a mixture of cyclohexyl bromide (72.8 wt%) and cis-decalin (27.2 wt%), saturated with tetrabutylammonium bromide (TBAB) ($\epsilon_p \approx 5.6$), to guarantee near-refractive index and density matching [54,55]. The final suspensions are equilibrated in the stock vial for 8 days, followed by another 3 days in the electric bottle sample cell, before turning the electric field on (frequency $f = 1$ MHz). Different compression protocols are achieved by varying the intensity of the electric field ($E_{\text{rms}} = 0.2, 0.25, \text{ or } 0.3$ V/ μm). Hence, we gradually increase the particle concentration by compression at constant stress, which entails a variable rate, starting from typically ~ 20 wt%. The structural evolution is resolved using confocal microscopy (Supplemental Material Fig. 3 [41]).

The experiments on the colloidal system are compared to molecular dynamics simulations of a model binary atomistic system described by pairwise potentials, optimally parametrized for the experimental systems. As the physics of bond frustration is mostly determined by the near-range inter-particle repulsion [57], we employ a modified version of the Wahnström Lennard-Jones (LJ) potential [58] whose

bonding energy depends explicitly only on particle size. Instantaneous configurations of both the undercooled liquid and the amorphous solid regime are obtained through a linear temperature quench from a well-equilibrated high temperature liquid at fixed zero pressure. Three different quench rates, spanning up to 3 orders of magnitude, are used: $\dot{T}_n = \dot{T}_0/10^n$, with $n = 1, 2, 3$. Details of the LJ parametrization and the simulations are given in Supplemental Material Sec. E [41].

The local structural motifs, classified into local bonding classes enumerated by Nelson [34], are identified in both experimental and simulated systems using a modified Voronoi tessellation [39,59], by labeling the local environments via the triples (N_4, N_5, N_6) . Here N_n is the number of bonds of bond-order n . Two nearest-neighbor particles are identified as having a bond of order n if they have n common neighbors. Thus (0,12,0) represents the defect-free icosahedron, the minimally frustrated structure associated with both a low local energy and volume [60,61]. Further details on the analysis are provided in Supplemental Material Secs. H–I [41].

Local structural motifs and mapping temperature for athermal experiments.—The local structural motifs in the experimental configurations achieved by compression of the colloidal systems are compared here to those in the simulated atomistic system, undergoing thermal quenching. In simulations, the glass transition regime manifests itself by a change in slope in the energy and volume per particle with respect to decreasing temperature (Supplemental Material Fig. 5 [41]), where the intersection of the low and high temperature linear extrapolations gives a well-founded estimate of the glass transition temperature T_g (Supplemental Material Fig. 7 [41]). At temperatures just above T_g , all curves for different \dot{T}_n progressively deviate from each other, indicating kinetic arrest and the transition to a structural glass. The slowest quench ($n = 3$) produces the lowest glassy cohesive energy and volume per particle, and hence the most relaxed structure. Correspondingly, the icosahedral or Frank-Kasper (IFK) fraction content increases with decreasing temperatures, as the system enters the glass transition regime (Supplemental Material Fig. 4 [41]). The slow quench rates (i.e., more relaxed glasses) have an increased IFK fraction. This agrees with earlier works showing that well-relaxed glassy structures consist of a kinetically arrested system-spanning network of small particle icosahedral motifs [62–64] penetrated by sixfold defect bonds associated with large particle Frank-Kasper structures [27], with the remaining regions consisting of fourfold, fivefold, and sixfold bonds [38]. On the other hand, in a deeply undercooled liquid regime, before the glass transition, the structure generally consists of nonpercolating icosahedral motives. Because of their topological origin, such low-energy structural motifs are rather insensitive to local distortions. Hence, they offer a platform to map the experimental colloidal systems onto the

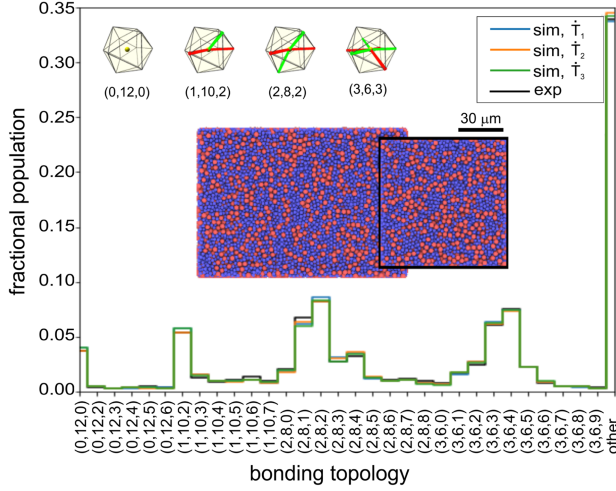


FIG. 1. Comparison of the local structural motifs populations normalized by the total particle number, for a colloidal experiment and atomistic simulations of a thermally quenched LJ system at the effective temperatures T_n^* , for different quench rates $\dot{T}_n = \dot{T}_0/10^n$, with $n = 1, 2, 3$. The system has $\alpha = 0.7$ and it is experimentally compressed with $E_{\text{rms}} = 0.25 \text{ V}/\mu\text{m}$ up to a volume fraction $\Phi \sim 0.52$. The inset depicts schematics of most frequently occurring bonding topologies, with green and red lines indicating bonds of order 4 and 6, respectively, and a planar view of experiments (left) and simulations at \dot{T}_3 (right).

simulated atomistic ones, revealing how relaxed the colloidal systems really are.

To map an instantaneous configuration of the colloidal system onto the thermal atomistic one, for each quench rate \dot{T}_n we determine an effective temperature T_n^* , based on the optimal quantitative matching of the experimental and simulated (N_4, N_5, N_6) populations, as defined by their minimum root-mean-square (rms) residual (Supplemental Material Fig. 6 [41]). The corresponding populations of local bonding motifs found in experiments and simulations at T_n^* are displayed in Fig. 1 and Supplemental Material Fig. 12 [41] for two different samples, revealing a remarkable agreement. The combination of the well-founded estimate of T_g from simulations with the mapping of the colloidal system on the atomistic one provides an internally consistent way of unifying colloidal and atomistic systems, although they are quenched in different ways.

Effect of compression protocol and composition.—We repeat the mapping procedure for consecutive configurations achieved during an experimental compression, to obtain a time-resolved mapping while approaching the glass transition for a system at a given composition $\chi_s = V_s/(V_s + V_l)$, where V_s and V_l are the total volumes of small and large particles, respectively. In the electric bottle experiment, suspensions undergo compression under a constant stress, possibly slightly reduced upon crowding. The inset in Fig. 2 displays the effective temperature as a function of the experimental volume fraction Φ for two continuous compression experiments, where time is an

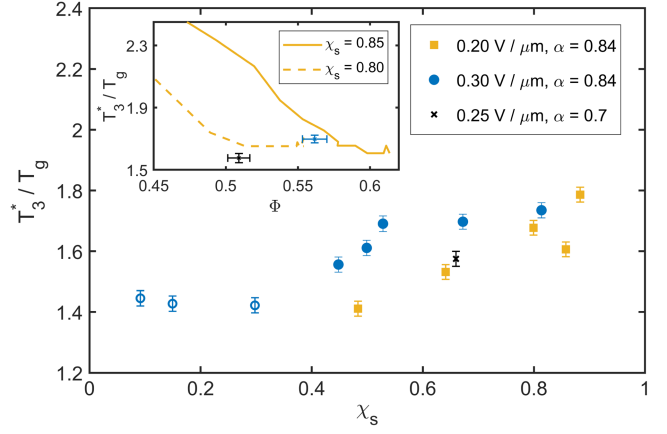


FIG. 2. Normalized effective temperature of compressed colloidal systems versus composition. The systems are compressed with $E_{\text{rms}} = 0.2$ (yellow), 0.25 (black), and $0.3 \text{ V}/\mu\text{m}$ (blue) for 5 day (solid symbols) or 52 h (open symbols). The inset depicts the evolution of the effective temperature versus volume fraction, during a compression, for systems with $\chi_s = 0.8$ (dashed line) and $\chi_s = 0.85$ (solid line). The two data points (blue and black) correspond to two different realizations at $\chi_s = 0.75$, for which we provide the detailed simulated dynamics (Supplemental Material Figs. 14 and 15 [41]). The error bars indicate the precision of the reported quantities, as derived from the temperature sampling in simulations and the typical experimental error for the considered particle polydispersity [56].

implicit variable. Over longer times, the curves level off and reach a plateau. This is attributed to a slowing down in structural rearrangements. Upon compression or upon quenching, an increasing number of low-energy structural motifs emerge (Supplemental Material Fig. 11 [41]), leading to increasing energy barriers for further structural evolution and prolonged relaxation times [60]. Our athermal experimental systems can only explore such motifs when the barrier energies are small enough to be overcome by stress-driven structural instabilities during constant stress compression in the experiments. Once these low-energy structural transitions become exhausted, the evolution becomes exceedingly slow, seemingly arrested within the experimental time frame. However, the mapping method enables verification of whether the system has effectively entered a glassy state. The volume fraction at which the plateau is reached in the experiments is approximately $\Phi_p \sim 0.5$ for $\chi_s = 0.8$ and $\Phi_p \sim 0.6$ for $\chi_s = 0.85$, with initial volume fraction of 0.25 and 0.3, respectively. Notably, even a minor composition variation of 6% results in a more than 15% variation in Φ_p . This variation exceeds typical experimental uncertainties in volume fraction measurement, which are around 3% [56]. Therefore, we conclude that, for a given compression protocol, Φ_p also depends on the initial volume fraction, in line with previous findings [65], while the mapping temperature of the final slowed-down state primarily depends on the composition χ_s .

In Fig. 2, we display the normalized effective temperature T_3^*/T_g in the long-time plateau as a function of composition χ_s . The corresponding volume fractions are reported in Supplemental Material Fig. 8 [41]. These results were achieved by compressing for 5 days with field intensities $E_{\text{rms}} = 0.2 \text{ V}/\mu\text{m}$ (yellow) and $E_{\text{rms}} = 0.3 \text{ V}/\mu\text{m}$ (blue). Normalizing T_3^* with respect to T_g offers a quantifiable measure of proximity to the glass transition and, consequently, the relaxation of the colloidal system. As expected, the weaker hence slower compression (yellow) leads to lower effective temperatures T_3^*/T_g , indicating a closer proximity to the glass transition. The mapping temperature T_n^* weakly depends on the simulated quench rate, where faster quench rates correspond to lower T_n^* values (Supplemental Material Figs. 6 and 9 [41]). Such a weak dependence reflects the close-to meta-equilibrium state of the simulated undercooled liquid. By employing the mapping protocol, we can also incorporate results where the compression is halted after 52 h (represented by open circles) into an effective measure of the distance to the glass transition. Remarkably, all mapping temperatures are well above the corresponding glass transition temperature T_g , and thus in the meta-equilibrium of the simulated undercooled liquid. This observation is also confirmed by the fact that the corresponding simulated systems have not yet developed a caging plateau in the intermediate scattering function ISF [66] (Supplemental Material Fig. 14 [41]), nor a divergence in the dynamic viscosity η (Supplemental Material Fig. 15 [41]). Details of the calculation of the ISF and η are provided in Supplemental Material Sec. G [41]. For both compression protocols, the mapping temperature increases with the fraction of small particles χ_s . At increasing fractions of small particles several factors might hinder the overcoming of energy barriers: a larger contact area, entailing higher dissipation in over-damped dynamics, higher volume filling of the small particles *i.e.* higher crowding, and a differing heterogeneity. To additionally assess the role of particle sizes, we consider a system with particle diameters 2.1 and 3 μm , namely a ratio $\alpha = 0.7$, compressed with $E_{\text{rms}} = 0.25 \text{ V}/\mu\text{m}$ (black cross). Compared to the system with $\alpha = 0.84$, the mapping temperature in the arrested state is lower, indicating a greater degree of relaxation. We attribute this observation to the increased heterogeneity of the system with $\alpha = 0.7$. Higher degrees of heterogeneity are indeed associated to more unstable energy states, with more fluctuating energy landscapes favoring relaxation [67]. This is in line with previous numerical findings that localized stress-driven structural transitions (shear transformation zones [68]) can mediate plasticity in quasistatic loading protocols due to local volume and therefore stress heterogeneity. Hence heterogeneity can play the role of an effective temperature in an athermal amorphous solid [69].

Midrange icosahedral ordering.—The robustness of the icosahedral motif has long been appreciated at the

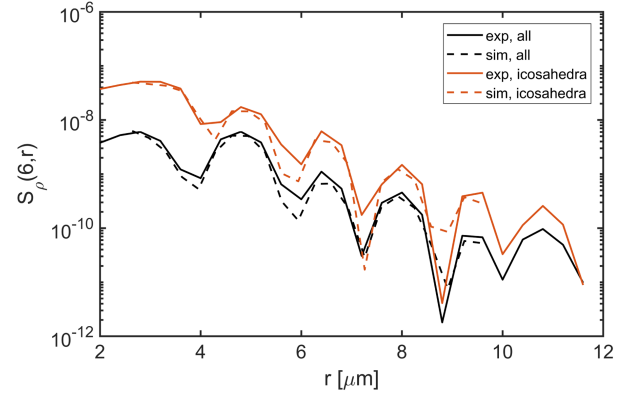


FIG. 3. Square root of the angular power spectrum $l = 6$ versus radial distance, for all particles (black) and for icosahedral-centered particles (red), in experiments (solid lines) and simulations (dashed lines), for the system of Fig. 1.

nearest-neighbors level and used to investigate the LFS structures of undercooled liquids [70–76]. Icosahedral symmetry has, however, also been used to evaluate midrange ordering. A recent probe exploits the spherical harmonic transform of a four-point spatial correlation function, where the $l = 6$ harmonic coefficient is found to dominate, indicating a non-negligible icosahedral point-like symmetry of liquid medium-range order [77,78]. Figure 3 and Supplemental Material Fig. 13 [41] display a similar analysis for two experiments and the corresponding simulations. The details of the analysis are described in Supplemental Material Sec. I [41]. In particular, we plot $S_\rho(l, r) = [(2l + 1)^{-1} \sum_{m=-l}^l |\rho_l^m(r)|^2]^{1/2}$ for $l = 6$ as a function of the radial distance r , with $\rho(r, \theta, \varphi) = \sum_{l=0}^{\infty} \sum_{m=-l}^l \rho_l^m(r) Y_l^m(\theta, \varphi)$ the particle density around a particle averaged over all such particles, decomposed with respect to the spherical harmonics $Y_l^m(\theta, \varphi)$, where θ, φ are the angular coordinates. We find a close agreement between the colloidal and model LJ system at the mapping temperature. If the particle at the origin has the icosahedral motif, the $S_\rho(6, r)$ increases by an order of magnitude, demonstrating the relevance of nonicosahedral motifs, but also the Frank-Kasper motifs which accommodate its defected packing. Such a structural indicator has been directly related to dynamic heterogeneities [78]. Therefore, the agreement in midrange ordering does not only confirm the validity of our mapping approach, but also suggests a direct link between the proposed local motif analysis and some dynamical aspects of the glass transition. It is important to underline that, while inertial and stochastic dynamics can give similar results in this temperature regime [22,23,79], the over-damped Brownian dynamics of our experimental system will give an entirely different timescale for arrest. Therefore, our structural mapping does not directly translate into a dynamic mapping of colloidal and atomistic systems. Still, it allows us to establish a meaningful baseline to study deviations from hard-sphere Brownian dynamics “at equal

structure,” which can be calculated as described in Supplemental Material Sec. G [41]. In colloidal systems such deviations are expected due to the presence of brush layer lubrication [80], hydrodynamics [81], hydrodynamics within the brush [82], softness [83] and noncentral or contact forces [84].

Conclusions.—A colloidal glass former, arrested by mechanically increasing the volume fraction and brought close to the glass transition, has been compared to a thermally quenched atomistic simulated LJ system. The striking similarity in the bonding topology distributions of local structural motifs provides a robust method for establishing a quantitative equivalence between particle volume fraction and temperature, eliminating experimental ambiguities. Specifically, this method demonstrates that our arrested colloidal systems exhibit structural similarities to deeply undercooled liquids, even at high volume fractions $0.58 \leq \Phi \leq 0.64$, where $\Phi = 0.58$ is typically considered the glass transition limit for near-hard colloids [21] and $\Phi = 0.64$ the maximum random packing fraction [85]. The consistency of our approach is evident in the excellent agreement between mapped thermal and athermal systems, particularly regarding midrange ordering, assessed by deviations from icosahedral point-group symmetry. These deviations, stemming from the connectivity of local structural motifs [29], are closely linked to dynamical heterogeneities [78]. Overall, we provide a way to unambiguously determine how close to the glass transition a colloidal system is by quantitatively assessing its relaxation.

We thank Prof. André Studart’s lab (ETH, Zürich) for allowing us to access the confocal microscope and electric field setups, in particular, Marco Binelli (ETH, Zürich) for his support with the experimental setup. We are thankful to Johan Stiefelhagen (Utrecht University) and Andrew Schofield (University of Edinburgh), who kindly provided the colloidal particles. J. V. acknowledges the late W. R. Russel (Princeton University) for illuminating discussions. We acknowledge financial support from the Swiss National Science Foundation SNSF (Project No. 192336).

*laura.stricker@mat.ethz.ch

†peter.derlet@psi.ch

- [1] W. C. K. Poon, Colloids as big atoms, *Science* **304**, 830 (2004).
- [2] S. Auer and D. Frankel, Prediction of absolute crystal-nucleation rate in hard-sphere colloids, *Nature (London)* **409**, 1020 (2001).
- [3] E. R. Weeks, J. C. Crocker, A. C. Levitt, A. Schofield, and D. A. Weitz, Three-dimensional direct imaging of structural relaxation near the colloidal glass transition, *Science* **287**, 627 (2000).
- [4] K. N. Pham, A. M. Puertas, J. Bergenholtz, S. U. Egelhaaf, A. Moussaïd, P. N. Pusey, A. B. Schofield, M. E. Cates,

- M. Fuchs, and W. C. K. Poon, Multiple glassy states in a simple model system, *Science* **296**, 104 (2002).
- [5] E. M. Terentjev, *The Oxford Handbook of Soft Condensed Matter*, edited by E. M. Terentjev and D. A. Weitz (Oxford University Press, Oxford, 2015).
- [6] J. K. G. Dhont, *An Introduction to Dynamics of Colloids*, 2nd ed. (Elsevier, Amsterdam, 2003).
- [7] U. Bengtzelius, W. Götze, and A. Sjölander, Dynamics of supercooled liquids and the glass transition, *J. Phys. C* **17**, 5915 (1984).
- [8] P. N. Pusey and W. van Meegen, Phase behaviour of concentrated suspensions of nearly hard colloidal spheres, *Nature (London)* **320**, 340 (1986).
- [9] P. N. Pusey and W. van Meegen, Observation of a glass transition in suspensions of spherical colloidal particles, *Phys. Rev. Lett.* **59**, 2083 (1987).
- [10] M. Von Smoluchowski, Versuch einer mathematischen Theorie der Koagulationskinetik kolloider Lösungen, *Z. Phys. Chem.* **92**, 129 (1917).
- [11] E. J. W. Verwey, F. de Boer, and J. H. Vansanten, Cation arrangement in spinels, *J. Chem. Phys.* **16**, 1091 (1948).
- [12] M. Y. Lin, H. M. Lindsay, D. A. Weitz, R. C. Ball, R. Klein, and P. Meakin, Universality in colloid aggregation, *Nature (London)* **339**, 360 (1989).
- [13] S. Asakura and F. Oosawa, Interaction between particles suspended in solutions of macromolecules, *J. Polym. Sci.* **33**, 183 (1958).
- [14] G. Brambilla, D. El Masri, M. Pierno, L. Berthier, L. Cipelletti, G. Petekidis, and A. B. Schofield, Probing the equilibrium dynamics of colloidal hard spheres above the mode-coupling glass transition, *Phys. Rev. Lett.* **102**, 085703 (2009).
- [15] O. S. Narayanaswamy, A model of structural relaxation in glass, *J. Am. Ceram. Soc.* **54**, 491 (1971).
- [16] J. C. Mauro, Y. Yue, A. J. Ellison, P. K. Gupta, and D. C. Allan, Viscosity of glass-forming liquids, *Proc. Natl. Acad. Sci. U.S.A.* **106**, 19780 (2009).
- [17] R. Juárez-Maldonado and M. Medina-Noyola, Theory of dynamic arrest in colloidal mixtures, *Phys. Rev. E* **77**, 051503 (2008).
- [18] F. Turci, C. P. Royall, and T. Speck, Non-equilibrium phase transition in an atomistic glassformer: The connection to thermodynamics, *Phys. Rev. X* **7**, 031028 (2017).
- [19] W. Götze, *Complex Dynamics of Glass-Forming Liquids* (Oxford University Press, Oxford, 2009).
- [20] E. Bouchbinder and J. S. Langer, Linear response theory for hard and soft glassy materials, *Phys. Rev. Lett.* **106**, 148301 (2011).
- [21] G. L. Hunter and E. R. Weeks, The physics of the colloidal glass transition, *Rep. Prog. Phys.* **75**, 066501 (2012).
- [22] T. Gleim, W. Kob, and K. Binder, How does the relaxation of a supercooled liquid depend on its microscopic dynamics?, *Phys. Rev. Lett.* **81**, 4404 (1998).
- [23] G. Szamel and E. Fleener, Independence of the relaxation of a supercooled fluid from its microscopic dynamics: Need for yet another extension of the mode-coupling theory, *Europhys. Lett.* **67**, 779 (2004).
- [24] E. R. Weeks and D. A. Weitz, Properties of cage rearrangements observed near the colloidal glass transition, *Phys. Rev. Lett.* **89**, 095704 (2002).

- [25] G. Tarjus, S. A. Kivelson, Z. Nussinov, and P. Viot, The frustration-based approach of supercooled liquids and the glass transition: A review and critical assessment, *J. Phys. Condens. Matter* **17**, R1143 (2005).
- [26] C. P. Royall, A. Malins, A. J. Dunleavy, and R. Pinney, Strong geometric frustration in model glassformers, *J. Non-Cryst. Solids* **407**, 34 (2015).
- [27] F. C. Frank and J. S. Kasper, Complex alloy structures regarded as sphere packings. I. definitions and basic principles, *Acta Crystallogr.* **11**, 184 (1958).
- [28] F. C. Frank and J. S. Kasper, Complex alloy structures regarded as sphere packings. II. Analysis and classification of representative structures, *Acta Crystallogr.* **12**, 483 (1959).
- [29] D. R. Nelson, *Defects and Geometry in Condensed Matter Physics* (Cambridge University Press, New York, 2002).
- [30] E. Flenner and G. Szamel, Fundamental differences between glassy dynamics in two and three dimensions, *Nat. Commun.* **6**, 7392 (2015).
- [31] U. R. Pedersen, T. B. Schröder, J. C. Dyre, and P. Harrowell, Geometry of slow structural fluctuations in a supercooled binary alloy, *Phys. Rev. Lett.* **104**, 105701 (2010).
- [32] C. R. Iacovella, A. S. Keysa, and S. C. Glotzer, Self-assembly of soft-matter quasicrystals and their approximants, *Proc. Natl. Acad. Sci. U.S.A.* **108**, 20935 (2011).
- [33] D. R. Nelson, Liquids and glasses in spaces of incommensurate curvature, *Phys. Rev. Lett.* **50**, 982 (1983).
- [34] D. R. Nelson, Order, frustration, and defects in liquids and glasses, *Phys. Rev. B* **28**, 5515 (1983).
- [35] P. M. Derlet, Correlated disorder in a model binary glass through a local SU(2) bonding topology, *Phys. Rev. Mater.* **4**, 125601 (2020).
- [36] J.-F. Sadoc, Amorphous structural models using regular tessellation of curved space, *J. Phys. (Paris), Colloq.* **41**, 326 (1980).
- [37] C. Donati, J. F. Douglas, W. Kob, S. J. Plimpton, P. H. Poole, and S. C. Glotzer, Stringlike cooperative motion in a supercooled liquid, *Phys. Rev. Lett.* **80**, 2338 (1998).
- [38] P. M. Derlet and R. Maass, Emergent structural length scales in a model binary glass—the micro-second molecular dynamics time-scale regime, *J. Alloys Compd.* **821**, 153209 (2020).
- [39] P. M. Derlet, H. Bocquet, and R. Maass, Viscosity and transport in a model fragile metallic glass, *Phys. Rev. Mater.* **5**, 125601 (2021).
- [40] M. T. Sullivan, K. Zhao, A. D. Hollingsworth, R. H. Austin, W. B. Russel, and P. M. Chaikin, An electric bottle for colloids, *Phys. Rev. Lett.* **96**, 015703 (2006).
- [41] See Supplemental Material at <http://link.aps.org/supplemental/10.1103/PhysRevLett.132.218202>, which includes Refs. [42–51] for additional information about the experimental methods, the numerical simulations and the performed analysis.
- [42] A. Yethiraj, Tunable colloids: control of colloidal phase transitions with tunable interactions, *Soft Matter* **3**, 1099 (2007).
- [43] P. M. Derlet and R. Maass, Thermal processing and enthalpy storage of a binary amorphous solid: A molecular dynamics study, *J. Mater. Res.* **32**, 2668 (2017).
- [44] J. Zemp, M. Celino, B. Schönfeld, and J. F. Löffler, Crystal-like rearrangements of icosahedra in simulated Copper-Zirconium metallic glasses and their effect on mechanical properties, *Phys. Rev. Lett.* **115**, 165501 (2015).
- [45] P. M. Derlet and R. Maass, Microplasticity in a fragile model binary glass, *Acta Mater.* **209**, 116771 (2021).
- [46] P. M. Derlet and R. Maass, Optimally rejuvenated model binary glasses, *Phys. Rev. Mater.* **6**, 125604 (2022).
- [47] A. P. Thompson, H. M. Aktulga, R. Berger, D. S. Bolintineanu, W. M. Brown, P. S. Crozier, P. J. in't Veld, A. Kohlmeyer, S. G. Moore, T. D. Nguyen, R. Shan, M. J. Stevens, J. Tranchida, C. Trott, and S. J. Plimpton, LAMMPS—a flexible simulation tool for particle-based materials modeling at the atomic, meso, and continuum scales, *Comput. Phys. Commun.* **271**, 108171 (2022).
- [48] M. S. Green, Markoff random processes and the statistical mechanics of timedependent phenomena. II. Irreversible processes in fluids, *J. Chem. Phys.* **22**, 398 (1954).
- [49] R. Kubo, Statistical-mechanical theory of irreversible processes I, *J. Phys. Soc. Jpn.* **12**, 570 (1957).
- [50] J.-Y. Tinevez, N. Perry, J. Schindelin, G. M. Hoopes, G. D. Reynolds, E. Laplantine, S. Y. Bednarek, S. L. Shorte, and K. W. Eliceiri, TrackMate: An open and extensible platform for single-particle tracking, *Methods* **115**, 80 (2017).
- [51] A. Stukowski, Visualization and analysis of atomistic simulation data with OVITO—the open visualization tool, *Model. Simul. Mater. Sci. Eng.* **18**, 015012 (2010).
- [52] G. P. Mikhailov and T. I. Borisova, Effect of monomer unit structure on molecular relaxation in stereospecific polymers, *Polym. Sci. USSR* **387**, 387 (1961).
- [53] G. Bosma, C. Pathmamanoharan, E. de Hoog, W. K. Kegel, A. van Blaaderen, and H. N. W. Lekkerkerker, Preparation of monodisperse, fluorescent PMMA-latex colloids by dispersion polymerization, *J. Colloid Interface Sci.* **245**, 292 (2002).
- [54] A. Yethiraj and A. van Blaaderen, A colloidal model system with an interaction tunable from hard sphere to soft and dipolar, *Nature (London)* **421**, 513 (2003).
- [55] H. R. Vutukuri, A. F. Demirörs, B. Peng, P. D. van Oostrum, A. Imhof, and A. van Blaaderen, Colloidal analogues of charged and uncharged polymer chains with tunable stiffness, *Angew. Chem., Int. Ed.* **51**, 11249 (2012).
- [56] W. C. K. Poon, E. R. Weeks, and C. P. Royall, On measuring colloidal volume fractions, *Soft Matter* **8**, 21 (2012).
- [57] D. Chandler and J. P. Garrahan, Dynamics on the way to forming glass: Bubbles in space-time, *Annu. Rev. Phys. Chem.* **61**, 191 (2010).
- [58] G. Wahnström, Molecular-dynamics study of a supercooled two-component Lennard-Jones system, *Phys. Rev. A* **44**, 3752 (1991).
- [59] See GitHub repository at <https://github.com/derlet/SU2> (2020).
- [60] F. C. Frank, Supercooling of liquids, *Proc. R. Soc. A* **215**, 43 (1952).
- [61] P. Chaudhari and D. Turnbull, Structure and properties of metallic glasses, *Science* **199**, 11 (1978).
- [62] H. Jónsson and H. C. Andersen, Icosahedral ordering in the Lennard-Jones liquid and glass, *Phys. Rev. Lett.* **60**, 2295 (1988).

- [63] H. W. Sheng, W. K. Luo, F. M. Alamgir, J. M. Bai, and E. Ma, Atomic packing and short-to-medium-range order in metallic glasses, *Nature (London)* **439**, 419 (2006).
- [64] E. Ma, Tuning order into disorder, *Nat. Mater.* **14**, 547 (2015).
- [65] S. R. Liber, S. Borohovich, A. V. Butenko, A. B. Schofield, and E. Sloutskin, Dense colloidal fluids form denser amorphous sediments, *Proc. Natl. Acad. Sci. U.S.A.* **110**, 5769 (2013).
- [66] D. R. Reichman and P. Charbonneau, Mode-coupling theory, *J. Stat. Mech.* (2005) P05013.
- [67] D. P. Wang, J. C. Qiao, and C. T. Liu, Relating structural heterogeneity to β relaxation processes in metallic glasses, *Mater. Res. Lett.* **7**, 305 (2019).
- [68] M. L. Falk and J. S. Langer, Deformation and failure of amorphous, solidlike materials, *Annu. Rev. Condens. Matter Phys.* **2**, 353 (2011).
- [69] M. L. Falk and J. S. Langer, Dynamics of viscoplastic deformation in amorphous solids, *Phys. Rev. E* **57**, 7192 (1998).
- [70] M. Celino, V. Rosato, A. Di Cicco, A. Trapananti, and C. Massobrio, Role of defective icosahedra in undercooled copper, *Phys. Rev. B* **75**, 174210 (2007).
- [71] M. Leocmach and H. Tanaka, Roles of icosahedral and crystal-like order in the hard spheres glass transition, *Nat. Commun.* **3**, 974 (2012).
- [72] J. Taffs, S. R. Williams, H. Tanaka, and C. P. Royall, Structure and kinetics in the freezing of nearly hard spheres, *Soft Matter* **297**, 297 (2013).
- [73] C. P. Royall and W. Kob, Locally favoured structures and dynamic length scales in a simple glass-former, *J. Stat. Mech.* (2017) 024001.
- [74] F. Turci, T. Speck, and C. P. Royall, Structural-dynamical transition in the Wahnström mixture, *Eur. Phys. J. E* **41**, 54 (2018).
- [75] H. Tanaka, H. Tong, R. Shi, and J. Russo, Structural order as a genuine control parameter of dynamics in simple glass formers, *Nat. Rev. Phys.* **1**, 333 (2019).
- [76] S. Winczewski, J. Dziedzic, and J. Rybicki, In-depth characterization of icosahedral ordering in liquid copper, *Comput. Mater. Sci.* **166**, 57 (2019).
- [77] H. Yuan, Z. Zhang, W. Kob, and Y. Wang, Connecting packing efficiency of binary hard sphere systems to their intermediate range structure, *Phys. Rev. Lett.* **127**, 278001 (2021).
- [78] N. Singh, Z. Zhang, A. K. Sood, W. Kob, and R. Ganapathy, Intermediate-range order governs dynamics in dense colloidal liquids, *Proc. Natl. Acad. Sci. U.S.A.* **120**, e2300923120 (2023).
- [79] P. Montero de Hijes, P. Rosales-Pelaez, C. Valeriani, P. N. Pusey, and E. Sanz, Brownian versus Newtonian devitrification of hard-sphere glasses, *Phys. Rev. E* **96**, 020602(R) (2017).
- [80] A. Nomura, K. Ohno, T. Fukuda, T. Sato, and Y. Tsujii, Lubrication mechanism of concentrated polymer brushes in solvents: Effect of solvent viscosity, *Polym. Chem.* **3**, 148 (2012).
- [81] J. de Graaf, W. C. K. Poon, M. J. Haughey, and M. Hermes, Hydrodynamics strongly affect the dynamics of colloidal gelation but not gel structure, *Soft Matter* **15**, 10 (2019).
- [82] K. Ohno, Colloidal crystals formed by polymer brush-afforded fine particles, *Polym. Chem.* **1**, 1545 (2010).
- [83] C. P. Royall, W. C. K. Poon, and E. R. Weeks, In search of colloidal hard spheres, *Soft Matter* **9**, 17 (2013).
- [84] H. T. Nguyen, A. L. Graham, P. H. Koenig, and L. D. Gelb, Computer simulations of colloidal gels: how hindered particle rotation affects structure and rheology, *Soft Matter* **16**, 256 (2020).
- [85] S. Li, J. Zhao, P. Lu, and Y. Xie, Maximum packing densities of basic 3D objects, *Chin. Sci. Bull.* **55**, 114 (2010).